CZU 621.391.81

OPTICAL AND RADIO SYSTEMS FOR INVESTIGATION OF THE IONOSPHERE

Eugeniu Plohotniuc (State University "Alecu Russo", Republic of Moldova)

The existing modern optical and radio systems which were successfully used for investigation of the main parametrees, various kinds of instabilities and irregularities of the ionospheric plasma are briefly described.

The quickly changing plasma density in the non-regular ionosphere during its perturbations considerably affects propagation of radio waves through it, finally, decreasing the quality and efficiency of wireless communications, land-satellite and satellite-satellite, including positioning of any subscriber, stationary or moving, located in areas of service. An increase in the efficiency of short-wave wireless communication is impossible without a permanent observation of nonlinear processes occurring in the perturbed ionospheric plasma and without taking into consideration radio traces parameters, i.e., the key parameters of ionospheric communication link.

The parameters and dynamical processes occurring in the non-regular ionosphere are possible to investigate using modern radiophysical methods based on different devices and radio systems, such as optical devices, incoherent scatter radars, Global Navigation Satellite Systems (GNSS), superDARN, and ionosondes/digisondes.

The artisle briefly describes the existing modern optical and radio systems which were successfully used for investigation of the main nonlinear characteristics of the ionospheric plasma, various kinds of its instabilities and the corresponding irregularities of plasma density at various latitudes of the ionosphere without entering into a technical description of devices and systems.

Here, we draw the reader`s attention to the possibilities of each corresponding device or system without going into technical details and schematical descriptions (which can be found in the referred literature), describing only their operation characteristics and possibilities to investigate natural and artificial ionospheric phenomena.

Optical Devices

Optical devices, such as photometric and spectrometric devices, digital All - Sky cameras, and TV complexes are used to investigate the atmospheric and ionospheric parameters and processes. These devices are successfully used separately or with radar systems and ionosondes, operating regularly in many places over the world, such as Alaska, Arecibo, Arequipa, Fairbanks, New Zealand, Peru and Puerto Rico, Russia, the North and South Poles [1-16].

For example, at *Arecibo Incoherent Scatter Radar System* (AISRS), an optical set of equipments includes two *Tilting-Filter Photometers*, an *Ebert-Fastie Spectrometer* with one-meter focal length, two pressure-scanned *Fabry-Perot Interferometers* each having six-inch diameter etalon plates and lidars. The set of optical devices used in investigations of the atmosphere and the ionosphere is presented in Table 1.

Photometers, combined with a set of optical filters, are used to measure the intensities of airglow emissions of the visible and near-infrared part of the optical spectrum [1, 2]. Specific filters are available at Arecibo to measure the airglow lines of various gases in the atmosphere, such as OH, O_2, O, O^+, N, N_2^+, H, He, and Na.

Tilting-Filter Photometers assembled at AISRS have the following parameters: a single channel with bandwidth (at the level of 3 dB) of 0.3 to 1.0nm (depending on the choice of interference filter). The programmable filter tilt is controlled by the stepping motors with 10° tilt range or approximately 2.5-nm scan range with field-of-view varied between 0.25^o and 5.0^o using selecting field stops.

Spectrometers are used to measure spectral blends of airglow emission bands at medium to high spectral resolution [3, 4]. The *Ebert-Fastie Spectrophotometer* arranged at AISRS has the following parameters: one-meter focal length with a bandwidth varied between 0.02nm to 1.0 nm. A programmable wavelength scanning takes place via stepping motors with maximum scan range limited to 100nm (anywhere between roughly 300nm and 900 nm) with variable field-of-view, which varies between 0.1^o and 9.0^o.

Interferometers are generally used to measure Doppler temperature and winds that originate in the *E-* and *F*-regions of the ionosphere, or to measure the spectral distribution and temporal variation of the hydrogen geocorona [5–7]. *Fabry-Perot Interferometers* at AISRS have the following parameters: each interferometer is with 1.2-meter focal length and 0.15-meter clear apertures with typical bandwidth of 0.001nm and free spectral range of 0.01nm. The wavelength change takes place via pressure scanning using pistons and choice of scanning gas of Ar, CO_2, or SF_6. The field-of-view depends on the choice of aperture size, but it is typically 0.25^o for 630nm observations. It also has He-Ne frequency stabilized laser for linewidth calibration and thermal control of etalon and prefilter.

The Optical Laboratories at AISRS have one *Doppler Rayleigh Lidar* and two *Resonance Fluorescence Lidars*. The *Doppler Rayleigh Lidar* is used to measure the Doppler shifts and widths of the spectrum of the laser light that is broadened and backscattered from the atmosphere and lower ionosphere from about 15 to 70-80 km of altitude and have the following parameters: Nd/YAG-based laser transmitter with the 24-W average power (with 100 MW in its peak) operating at 532 nm and at frequency of 40 Hz with the pulse width of 6ns. It has the 80-cm diameter Cassegrain telescope receiver. All the other details can be found in [8-16]. The corresponding scheme of this lidar is presented in Fig. 1.

Table 1.

Optical instruments used to investigate atmospheric parameters and processes

Instrument	Observed Item	Altitude	Mode
Photometer (Tiny Ionospheric Photometer)	The airglow lines of various gases in the atmosphere, such as OH, O_2, O, O^+, N, N_2^+, H, He, and others	Different altitudes of ionosphere	Horizontal distribution
Fabry-Perot Interferometer	Horizontal and vertical wind velocity, and temperature at airglow layers	Upper mesosphere, lower thermosphere (when quiet:85, 95, 250 km; when active:85, 120, 250 km)	Horizontal distribution, night (new moon phase)
Fourier transform infrared spectrometer	Trace constituents	Troposphere, lower stratosphere (10-30 km)	Vertical distribution, day
Rayleigh lidar	Winds, temperature	Stratosphere, lower mesosphere (30-80 km)	Vertical distribution, night
Multiwavelength lidar	Aerosol, cloud	Upper troposphere, lower stratosphere (5-40 km)	Vertical distribution, night
All-sky camera	Luminosity of airglow layer, atmospheric waves	Upper mesosphere, lower thermosphere (when quiet:85, 95, 250 km; when active:85,120, 250 km)	Horizontal distribution, night (new moon phase)
Aurora Web Camera	Aurora Live Image	Operates at different altitudes of ionosphere	Day and night

Temperature profiles observed by Rayleigh lidar and theoretical results obtained with CIRA-86 model are presented in Fig. 2.

Resonance Fluorescence Lidars (Alexandrite-laser based, and Dye-laser based) can measure various metallic species of the upper atmosphere and lower ionosphere between about 70 and 115*km* altitude. An *Alexandrite laser transmitter* can be set between 720 and 800*nm* with doubled frequency output between 360 and 400*nm*. It has a 3-W average power (with 0.5 MW at the power peak) operating at 770*nm* with operational frequency of 28 Hz and the pulse width of 200*ns*. A *Dye laser transmitter* is tunable between about 300*nm* and 800*nm* depending on the dye/solvent used, as well as on the sets of doubling and mixing crystals. It has 4W average power (with 20-MW peak power) operating at 589*nm* with a working frequency of 40 Hz and the pulse width of 5*ns*.

Fig. 1. Scheme of the Rayleigh-Doppler lidar.

Fig. 2. Temperature profiles at Poker Flat (Average: 4 km).

Fig. 3. The schematic diagram of all-sky camera: 1. mamiya all-sky lens; 2. telecentric collimating lens; 3. filter wheel assembly from Keo Consultants; 4. positive diopter lens and tube; 5. Canon 50-mm f/1.2 lens; 6. Varo image intensifier tube assembled with refocusing optics; 7. zoom lens; 8. Pulnix TM-745 CCD camera with NTSC video output.

Both lidar systems employ 80-*cm* diameter, point-able Cassagrain telescopes and gated photomultiplier tube detectors with low-altitude choppers. The results obtained by *Doppler Rayleigh Lidar* and *Resonance Fluorescence Lidar* are presented in [8–16].

Both lidar systems employ 80-*cm* diameter, point-able Cassagrain telescopes and gated photomultiplier tube detectors with low-altitude choppers. The results obtained by *Doppler Rayleigh Lidar* and *Resonance Fluorescence Lidar* are presented in [8–16].

Simultaneous imaging observations of several airglow layers are very important to study vertical propagation of atmospheric gravity waves, which is one of the main aspects in bubbles structures generation in the equatorial layer *F*.

Moreover, simultaneous observations of wind, temperature, and airglow images are needed to study the dynamics of short-period waves [17]. Figure 3 presents a schematic diagram showing one of the all-sky camera systems. The all-sky imagers that are used in the new Finnish all-sky cameras are manufactured by *KeoConsultants*. Each imager has telecentric and non-vignetting optics, and the field of view of the fish-eye lens is 180 degrees. The technical specifications of all-sky camera systems are presented in Table 2.

Table 2.

Technical specifications of all-sky camera systems

ITEM	DESCRIPTION
Fish-eye lens	Canon 15mm/F2.8
Additional optics	Telecentric lens elements
Filter wheel	7-position filter wheel for 2" filters
Filters	Interference filters, wavelengths 557.7nm, 427.8nm, and 630.0 nm (BW 2.0 nm)
Intensifier lens	Canon 85mm/F1.2
Image intensifier	Varo 25mm MCP Gen II Image Intensifier model 3603
Reimaging optics	Canon 100mm/F2
CCD camera lens	Fujinon 25mm/F0.85
CCD camera	Pulnix 765E, 756(H)x581(V)

The filter wheel can accomodate seven narrow bandwidth interference filters. In normal operation one filter holder is left "free" to be able to acquire nonfiltered images. Every station has three filters: green, blue, and red.

The faint images are intensified before the final image is acquired by the CCD camera (B&W) and digitised by the frame grabber card of the station computer. This intensification allows shorter exposure times with less expensive CCD cameras, and typically an exposure takes 500ms. Example of the auroral images, representing observations along a North-South meridian versus latitude and time periods are presented on Fig. 4a. This particular data example is taken from a test operation of the new Finnish digital *All - Sky Camera* operated at

Kiruna Observatory, Sweden. Figure 4b is an optical intensity map of the red auroral light at wavelength 630*nm* emitted by oxygen atoms.
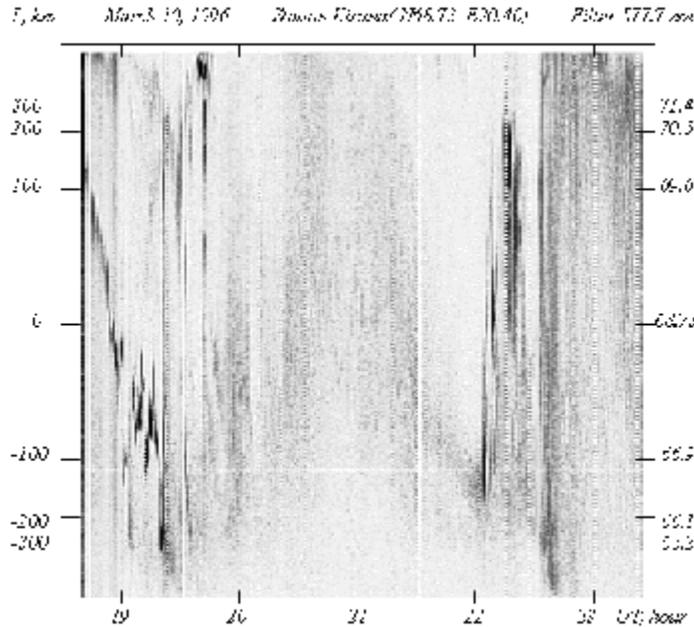

Fig. 4a. Example of an auroral Keogram, representing auroral observations along a north south meridian versus latitude and time (the scale is inverted, i.e. dark zones represent auroral emissions).
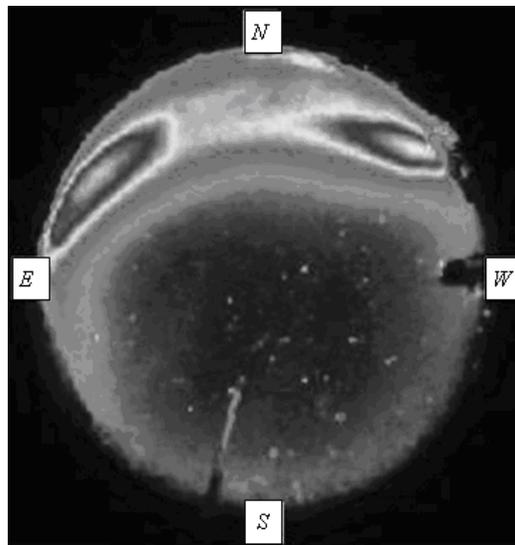

Fig. 4b. The false-colour intensity map of the red auroral light at wavelength 630 nm emitted by oxygen atoms.

Incoherent Scatter Radars

For ionospheric remote sensing from the ground the most refined and most modern equipment at present time is probably the incoherent scatter radar.

Incoherent Scatter Radar (ISR) is a technique for detecting and studying remote targets by transmitting a radio wave in the direction of the target, observing the reflection of the wave and providing direct information about electron densities, line-of-sight (LOS) drift velocities, the height of ionospheric layers and ratio electron and ion temperatures, T_e/T_i [18-35]. They also provide indirect measurements of a number of additional parameters, the most reliable of which is the neutral wind below ionospheric altitudes of 130*km*. The placements of incoherent scatter radars around the world are presented in Fig. 5.

Fig. 5. World incoherent scatter radars placements.

Initially, ISR systems were located at Arecibo and at Jicamarca. The Arecibo [18 - 20] and Jicamarca radars are both monostatic in nature (the transmitter and receiver are co-located).

The *Jicamarca Radio Observatory* was built in 1960-1961 by the Central Radio Propagation Laboratory of the National Bureau of Standards (see Fig. 6). The first incoherent scatter measurements at Jicamarca were made in 1961. The Jicamarca Radio Observatory is the premier scientific facility in the world for studying the equatorial ionosphere. The 49.92 MHz incoherent scatter radar is the principal facility of the Observatory. The radar antenna consists of a large square array of 18,432 half-wave dipoles arranged into 64 separate modules of 12 x 12 crossed half-wave dipoles. Each linear polarization of each module can be separately phased, and the modules can be fed separately or connected in almost any desired fashion. The isolation between the linear polarizations is very good, at least 50 dB, which is important for certain measurements.

An additional antenna module with 12x12 crossed dipoles was built in 1996. It is located 204*m* to the West of the West Corner of the main antenna and increases the lengths of the available interferometer base line to 564*m*.

There are three additional 50-MHz array antennas with steering up to +/-70° of zenith angles in the East-West direction only. Each consists of 4x2 half-wave dipoles mounted a quarter wavelength above a ground screen.

The *JULIA Radar* shares the main antenna of the Jicamarca Radio Observatory. JULIA is the abbreviation which stands for Jicamarca Unattended Long-term investigations of the Ionosphere and Atmosphere. It has an independent PC-based data acquisition system and makes use of some of the exciter stages of the Jicamarca Radar along with the main antenna array. Since this system does not use the main high-power transmitters, it can operate for a long period of time. With a pair of 30-kW peak power pulsed transmitters driving a 290*m* x 290*m* modular antenna array, JULIA is a formidable MST/coherent scatter radar. It is uniquely suited for studying day-to-day and long-term variability of equatorial plasma irregularities and neutral atmospheric waves, which until now have only been investigated episodically or in campaign mode.

Fig. 6. Jicamarca Radio Observatory.

The *Jicamarca Radio Observatory* has the following measurement capabilities [21 - 23]:

1) From all existing ISR-type radars, the *Jicamarca Radar* gives the most accurate measurements of drift velocity and electric field in the equatorial ionosphere. This is because of its unique equatorial geometry. Pointing perpendicular to the magnetic field makes it possible to measure line-of-sight (LOS) drift velocities with accuracy of the order of 0.5 *m/s*. Vertical *F*-region plasma drifts measured with such an accuracy allows to obtain information about zonal (e.g., equatorial) electric field with accuracy of about 12 *µV/m*. By studying the variation of drift velocity with altitude, up to 800-1000*km* (or perhaps even higher), it is possible to study the electrodynamics of the entire low-latitude ionosphere, up to the anomaly latitudes, because the electric field maps along the geomagnetic field lines.

2) The Jicamarca Radar also has a unique capability to probe the ionosphere up to very high altitudes. Because of the long radar wavelength, the incoherent scatter is not affected by problems of the Debye length at low electron

densities, and usable signals can be obtained from altitudes of 5000km and higher, giving densities and perhaps temperatures (but not drifts, since the beam cannot be simultaneously pointed perpendicular to **B**).

3) Absolute *F*-region measurements of electron density were performed by the Jicamarca Radar using Faraday rotation. Electron and ion temperatures and ion compositions were obtained with a double pulse technique that generates the signal auto-correlation function (ACF). Pulses are transmitted using orthogonal polarization to reduce clutter.

4) The Jicamarca Radar is the most sensitive radar in the world. Thus, it is capable of probing even the "gap" region near 45-50km, partly because of its long wavelength and partly because it has the largest power-aperture product compared with any other VHF radar.

The construction of the *Arecibo Radio Observatory* began in the summer of 1960. At present, the Arecibo Observatory has selected a data on ionospheric parameters, processes and phenomena over the 1966-2007 periods. We do not enter in detailed description of Arecibo Radio Observatory because of the wide spectrum of devices and systems arranged there. The reader can find all technical details in the corresponding literature [18-20].

The next generations of incoherent scatter radars (ISR) comprise some of the most advanced radar systems in the world. The best among these are the Millstone Hill and Sondre Strømfjord [27] radars in the American sector and the EISCAT radars (the European Incoherent SCATter Association) in Northern Scandinavia [24 – 26, 32, 33].

The *Millstone Hill Radar System* consists of two antennas of 25m and 68m radius, the operating frequencies for which are 1295 MHz and 440 MHz, respectively. The 68-m dish is fixed in the vertical direction, while the 25-m dish has full steerability in the azimuth and elevation domains. The peak powers are 3 MW for the 68-m dish and 4 MW for the 25-m dish.

Further, incoherent scatter radar, having a 27-m receiver dish and operating at a frequency of 1300 MHz, was developed at Stanford Research Institute, California, during the sixties. This radar, also a steerable monostatic pulsed facility like the smaller of the Millstone Hill system, was subsequently moved to Chatanika, Alaska, where it carried out some ground-breaking observations of the high-latitude ionosphere during the seventies [27- 30], before being moved again to Sondre Strømfjord, Greenland, where it is presently located.

The *EISCAT Radars*, located in Northern Scandinavia and on the Svalbard Archipelago, are currently at the leading edge of incoherent scatter system development. EISCAT is an international collaboration involving the research groups from France, Germany, Finland, Norway, Sweden, the United Kingdom and Japan (which joined this Association in 1996). EISCAT operates using three independent incoherent scatter radar systems: a tristatic UHF "mainland" system, with a transmit/receiver system located at Tromsø, Norway and receiver-only facilities located at Kiruna, Sweden and Sodankylä, Finland.

A new monostatic UHF radar (the EISCAT Svalbard Radar or ESR, [26]) is operated close to Longyearbyen, Svalbard. In addition, a monostatic VHF radar is located at Tromsø. All of these radars are pulsed systems, capable of a very wide range of different transmitter modulations and with the most advanced signal processing capabilities for any system of this kind. The mainland UHF system commenced operations in 1981, and the first results from the VHF were obtained in 1985, which is described in detail in Chapters 6 and 7. The EISCAT Svalbard Radar began operations on March 15 1996. The ESR is UHF radar operating at frequencies around 500 MHz with a 10 MHz bandwidth. The antenna is a Cassegrain-fed dish, similar to the dishes used by the mainland UHF radar system. All signal processing operations are performed digitally, so that much of the analogue hardware found for other types of ISR is not required for the ESR.

A *mainland UHF radar* system operates at frequencies close to 933 MHz, with sixteen different frequencies being available at 0.5 MHz intervals. The system comprises three fully steerable dishes of 32-*m* diameter. Transmission, reception and signal sampling are controlled with microsecond accuracy and a dedicated digital correlator exists to form ACFs.

A *VHF-radar* antenna is a cylindrical in the cross-section plane with the dimensions 120*m* x 40*m*. This antenna can only be moved in the elevation domain. Transmission and reception can also be carried out independently on the two halves of the antenna, allowing the VHF to provide a dual beam capability. The operating frequency of the VHF is 224 MHz, and the bandwidth availablity is the same as in the *UHF-radar* (16 frequencies separated by 0.5 MHz).

The new system, known as EISCAT_3D, will retain the unique and powerful multi-static configuration of the mainland EISCAT UHF-system. Phased-array technology will be employed throughout. The design goals include more precise temporal and spatial resolution of the observed data, an extension of the instantaneous measurements of full-vector ionospheric drift velocities from a single point to the entire altitude range of the radar, and built-in interferometric capabilities. For optimal performance in conditions of low-density plasma, and for the middle-latitude ionosphere, a frequency in the high VHF band (~240 MHz) will be used. The facility will provide high-quality ionospheric parameters measured in real time, as well as near-instantaneous response capabilities for researchers who need data to study unusual and unpredictable disturbances and phenomena occurring in high-and middle-latitude ionosphere. The geographic coordinates of incoherent scatter radars are given in Table 3.

To complete the survey of incoherent scatter radars currently operating around the world, we should mention the two systems in the former Soviet Union at Kharkov and Irkutsk, which are capable only of simple long pulse operation.

The long-term ISR observations provide an extremely valuable data about the ionosphere. The EISCAT Scientific Association, as an international research organisation operating with three geophysical research Incoherent Scatter Radar systems, with an Ionospheric Heater located in Northern Scandinavia, has a data basis for the 1997-2007 period. The EISCAT TromsøRadar system collected data

during the period of 1984-2007, the St.Santin Radar system (France, 44.6N, 2.2E) during 1973-1986, the Millstone Hill Radar during 1970-2007, the Arecibo Radar during 1966-2007, the Shigaraki Middle and Upper atmosphere Radar (MU Radar, Japan, 34.8N, 136.1E) during 1986-2003 [27], and the Sondrestrøm Radar during 1990-2007 [31-35].

Table 3.

Geographic coordinates of incoherent scatter radars

Station	Latitude	Longitude	Altitude (km)	Invariant latitude*	Country
ARECIBO	18.34500°	293.24700°	0.00000	32.17857°	Puerto Rico
EISCAT TROMSØRADAR	69.58300°	19.21000°	0.03000	66.40458°	Troms in Norway, Kiruna in Sweden and Sodankyl in Finland (Scandinavia)
SVALBARD RADAR (ESR)	78.09000°	16.02000°	0.43400	74.87426°	Scandinavia
IRKUTSK	52.17000°	104.45000°	0.45500	45.89960°	Russia
JICAMARCA	-11.95000°	283.13000°	1.50000	13.90181°	Peru
KHARKOV	50.00000°	36.20000°	0.00000	45.75379°	Ukraine
MILLSTONE	42.61950°	288.50827°	0.14600	53.40967°	USA
MU	34.80000°	136.10000°	0.00000	24.51836°	Japan
SONDRE STROMFJORD	67.00000°	309.00000°	0.00000	73.17249°	Greenland

* Calculations of the invariant latitude are unstable near the equator.

The scientific purpose of the measurements is to determine the radar operating modes. Different transmitted pulse schemes are used, depending on the need for range resolution, signal strength, time resolution, and frequency resolution. The rapid steering capability of the radar antenna allows to measure not just range, but also latitude and local time. Because of the many data-taking options, there are many ways to display data.

Finishing this paragraph, we present below only a few examples of the results obtained with Sondrestrøm Radar (see also details on the website: *http://isr.sri.com/iono/issdata.html*).

Thus, Fig. 7 is a typical display of data from a 120° elevation scan in the plane of the magnetic meridian. The vertical axis shows altitude from ground level to 600*km* and the horizontal axis shows 1000*km* of ground range from the South (at the left of the image) to the North (at the right of the image). From left to right and

from top to bottom this figure shows color-shaped electron density, electron temperature, and ion temperature and ion velocity in LOS conditions.
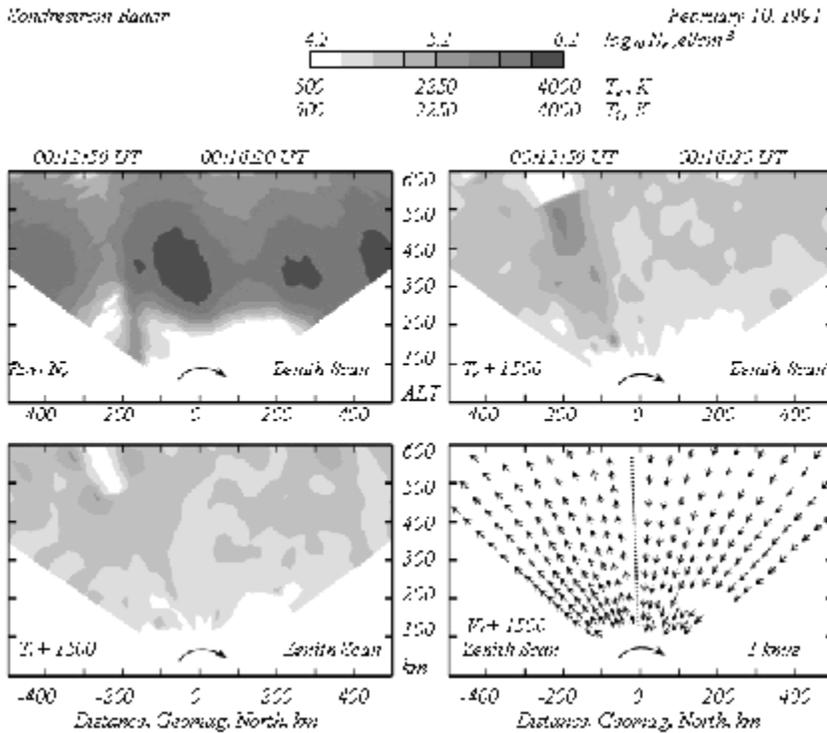

Fig. 7. Data from a 120° elevation scan in the plane of the magnetic meridian.

Figure 8 shows the radar data from a single 3-*min* integration with the antenna pointing parallel to the local magnetic field. Some of the basic parameters derived from radar records are electron density (N_e), ion drift velocity (V_i), and electron and ion temperatures (T_e and T_i). All of these quantities are obtained as a function of distance along the radar beam. Because this experiment was studying the E-region (where plasma parameters vary relatively rapidly with position), the pulse pattern used has 3 km range resolution.

In Fig. 9, the variation of electron density is shown as a function of altitude and time for a two-hour period in March of 1992. Because of the large scale heights in the *F*-region, a 48-*km* pulse was used. This provided greater signal strength and higher time resolution.

The variations in electron density (Fig. 10a) and ion drift velocities (Fig. 10b) as a function of latitude and time for a fixed altitude ($300km$) over a 24-hour period of observations during May, 1996 demonstrate the steering capability of the antenna and show measurements as a function of latitude. The radar sits under a doughnut-shaped band of data at 74° invariant latitude. The data are displayed North and South of the radar as the site rotates with Earth.
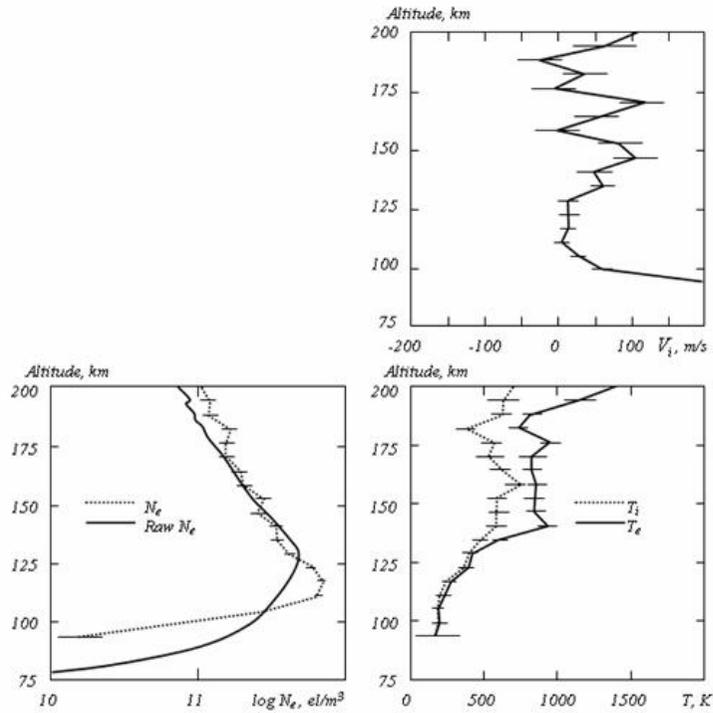
Fig. 8. The electron density (N_e), ion velocity (V_i), and electron and ion temperatures (T_e and T_i) as a function of distance along the radar beam.
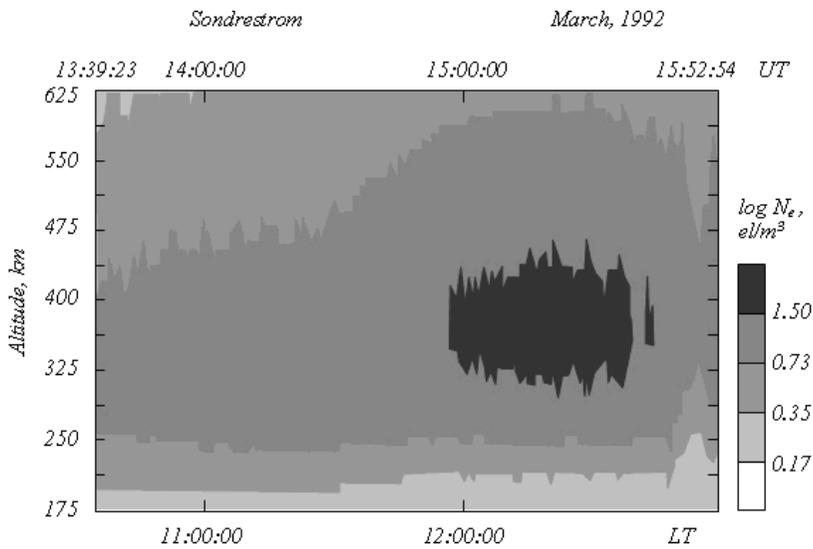
Fig. 9. The variation of electron density as a function of altitude and time for a two hour period in March of 1992.
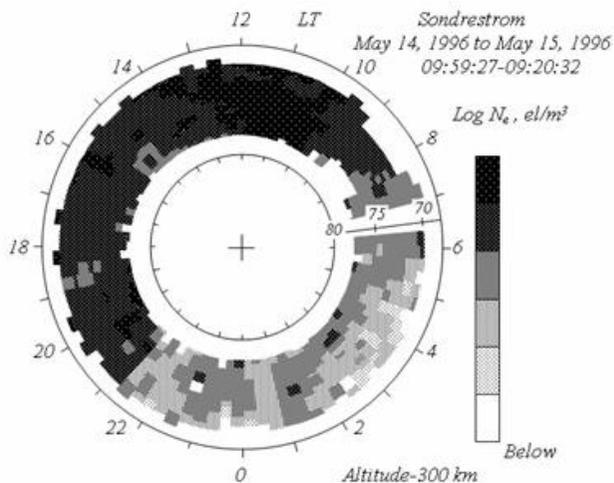
Fig. 10a. This clock dial plot displays the variations in electron density as a function of latitude and time for a fixed altitude (300 km) over a 24 hour period in May of 1996.
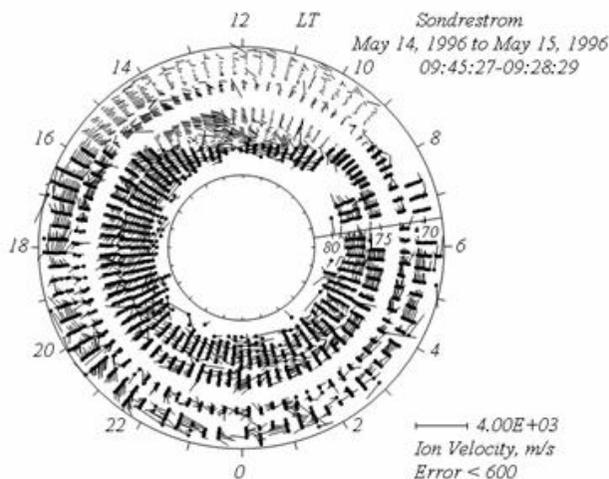
Fig. 10b. This figure displays ion drift velocities from the same time period as figure 10a.

SuperDARN

The *SuperDARN* network (Super Dual Auroral Radar Network [36]) is an international system for the studying of the Earth's upper troposphere, ionosphere, and their connections with the magnetosphere and outer space surrounding the Earth, which currently consists of a set of radars in the northern and in the southern hemispheres (see Table 4 and Fig. 11).

The construction of all the radars is roughly identical, with some minor differences in antenna design to accommodate the physical conditions at the site (see Fig. 12). Each of the radars has two arrays of antenna towers, the primary array consists of sixteen towers, and the secondary, interferometer array, consists of four towers. A phasing matrix attached to the antenna array is used to form the beam and to electronically steer the radar into one of sixteen different beam

directions. The radar transmits a short sequence of pulses in the HF-band and samples the echoe-signals arriving from the ionosphere.
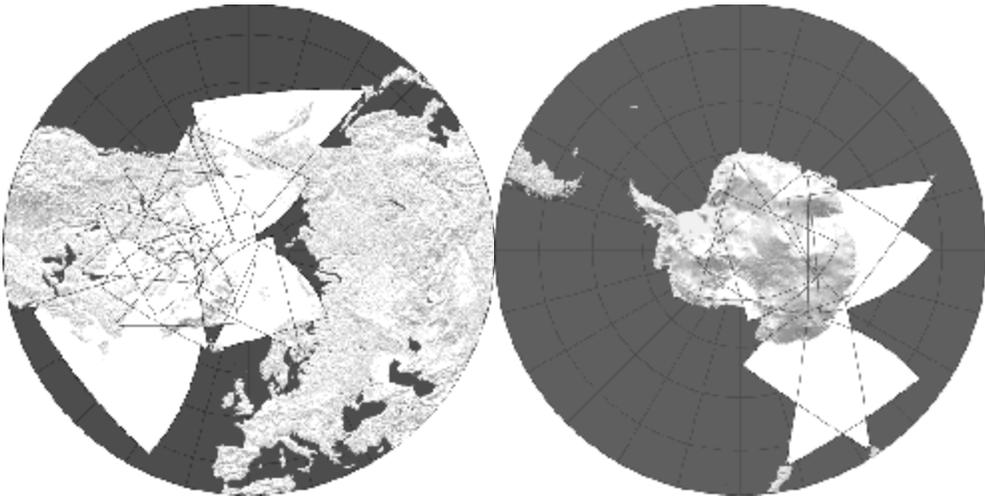

Fig. 11. Northern and Southern hemispheres of the SuperDARN international system.

Fig. 8.12. The Halley Bay station.

A sequence of pulses, referred to as a multi-pulse sequence, is carefully designed to allow the Doppler characteristics of different targets to be determined at multiple ranges by using the Auto-Correlation Function (ACF) of the received samples. Many sequences are transmitted and the calculated ACFs integrated over a period of several seconds to minimize the effect of noise. The final average ACF is then used to calculate back-scattered power, spectral width and Doppler velocity of the plasma density irregularities in non-regular ionosphere. In a standard operating mode, a multi-pulse sequence (of 7 pulses) is transmitted and sampled to resolve 75 ranges with a 45-*km* separation [37–42].

Table 4

The SuperDARN network

Station	Geographic coordinates	AAGM magnetic	Status of work	Location	Principal investigator
1	2	3	4	5	6
NORTHERN HEMISPHERE					
Rankin Inlet	62.82º N, 93.11º W	72.96º N, 28.17º W	24 hr/day	Nanavut, CANADA	Institute of Space and Atmospheric Studies University of Saskatchewan, Saskatoon, CANADA
King Salmon	58.68º N, 156.65º W	57.43º N, 100.51º E	24 hr/day	Alaska, USA	Communications Research Laboratory, Tokyo, Japan
Kodiak	57.60º N, 152.2º W	57.17º N, 96.28º W	24 hr/day	Kodiak Island, Alaska, USA	Geophysical Institute University of Alaska Fairbanks,USA
Prince George	53.98º N, 122.59º W	59.88º N, 65.67º W	24 hr/day	British Columbia, CANADA	Institute of Space and Atmospheric Studies University of Saskatchewan, Saskatoon, CANADA
Saskatoon	52.16º N, 106.53º W	61.34º N, 45.26º W	24 hr/day	Saskatoon, CANADA	Institute of Space and Atmospheric Studies University of Saskatchewan, Saskatoon, CANADA
Kapuskasin	49.39º N, 82.32º W	60.06º N, 9.22º W	24 hr/day	Ontario, CANADA	Johns Hopkins Applied Physics Laboratory, Laurel,USA
Goose Bay	53.32º N, 60.46º W	61.94º N, 23.02º E	24 hr/day	Goose Bay, CANADA	Johns Hopkins Applied Physics Laboratory, Laurel,USA

1	2	3	4	5	6
Stokkseyri	63.86º N, 22.02º W	65.04º N, 67.33º E	24 hr/day	Stokkseyri, ICELAND	LPCE/CNRS Orleans, FRANCE
Þykkvybaer	63.86º N, 19.20º W	64.59º N, 69 .65º E	24 hr/day	Þykkvybaer, ICELAND	Department of Physics, University of Leicester, ENGLAND
Hankasalmi	62.32º N, 26.61º E	59.78º N, 105.53º E	24 hr/day	Hankasalmi, FINLAND	Department of Physics, University of Leicester, ENGLAND
Wallops Island	37.93º N, 75.47º W	30.63º N, 75.52º E	24 hr/day	Wallops Island, Virginia, USA	Johns Hopkins Applied Physics Laboratory, Laurel,USA
Hokkaido	43.53º N, 143.61º E	38.14º N, 145.67º W	24 hr/day	Hokkaido, JAPAN	Solar-Terrestrial Environment Laboratory, Nagoya University, JAPAN
SOUTHERN HEMISPHERE					
Halley	75.52º S, 26.63º W	61.68º S, 28.92º E	24 hr/day	Halley Station, Antarctica	British Antarctic Survey High Cross, Cambridge, ENGLAND
Sanae	71.68º S, 2.85º W	61.52º S, 43.18º E	Began Operation in February, 1997	Sanae, Antarctica	School of Physics,University of KwaZulu-Natal, Durban, SOUTH AFRICA
Syowa South	69.00º S, 39.58º E	55.25º S, 23.00º E	24 hr/day	Syowa, Antarctica	National Institute of Polar Research, Tokyo, JAPAN
Syowa East	69.01º S, 39.61º E	55.25º S, 22.98º E	24 hr/day	Syowa, Antarctica	National Institute of Polar Research, Tokyo, JAPAN
Kerguelen	49.35º S, 70.26º E	58.73º S, 122.14º E	24 hr/day	Kergeulen, Island	LPCE/CNRS, Orleans, FRANCE

1	2	3	4	5	6
Tiger	43.38º S, 147.23º E	55.31º S, 133.36º W	24 hr/day	Tasmania	Department of Physics, La Trobe University Bundoora, AUSTRALIA
Tiger Unwin	46.51º S, 168.38º E	55.15º S, 106.54º W	24 hr/day	Unwin,New Zealand	Department of Physics, La Trobe University Bundoora, AUSTRALIA

The operation of a Radar is controlled by the Radar Operating System (ROS), which is responsible for controlling the Radar hardware, data processing, and data analysis and storage. A "Radar Control Program" defines the overall mode of the radar, including the operating frequency, integration period, range separation and the beam pattern used.

By combining the LOS measurements from a number of radars, the *SuperDARN* system can produce a two dimensional (2-D) pattern of the ion drifts. The advantages of the system are: an increasingly good coverage in both hemispheres, although southern hemisphere coverage is less developed; direct, accurate measurement of an important coupling parameter; and the rapid temporal coverage. The greatest weakness of the system is that many of its problems are exacerbated during times of high geomagnetic activity (e.g., magnetic storms). Therefore, *SuperDARN* radars should be an important component of validation, but should be used in conjunction with other data sources.

The Global Positioning System in Investigations of the Ionosphere

The Global Positioning System (GPS) is the autonomy functional Global Navigation Satellite System (GNSS). It consists of up to 24 medium Earth's orbit satellites in six different orbital planes, with the exact number of satellites varying as older satellites are retired and replaced. These satellites are travelling at speeds of roughly 7,000 miles an hour. Transmitter power is only 50*W* or less. Operational since 1978 and globally available since 1994, GPS is currently a most utilized satellite navigation system in the world.

Developed by the United States Department of Defense, it is officially named NAVSTAR GPS. GPS was originally intended for military applications, but then, from 1983, the system has become available for civilian use.

GPS has become a widely used aid to navigation worldwide, and a useful tool for map-making, land surveying, commerce, and scientific uses. GPS also provides

a precise time reference used in many applications including scientific study of earthquakes, and synchronization of telecommunications networks. A GPS receiver must be locked on to the signal of at least three satellites to calculate a 2-D position (latitude and longitude) and track any movements of subscribers. With four or more satellites in view, the receiver can determine the 3-D position of any subscriber (e.g., latitude, longitude and altitude). Once the user's position has been determined, the GPS unit can calculate other information, such as speed, bearing, tracking, trip distance, distance to destination, sunrise and sunset time and more.

GPS satellites transmit the following radio signals: military – 1227.6 MHz; civilian L1 – 1575.42 MHz; civilian L2 – 1227.60 MHz; nuclear burst detection L3 – 1381.05 MHz; telemetry on 2227.5 MHz (see details in *http://www.tbs-satellite.com/tse/online/prog_gps_freq.html*). Beginning from around 2008, civilians will have access to three GPS signals: L1 – 1575.42 MHz, L2 – 1227.60 MHz and L5 – 1176.45 MHz [43].

A GPS radio signal contains three different bits of information: a *pseudorandom code*, *ephemeris data* and *almanac data*. The *pseudorandom code* is simply a code that identifies which satellite transmits information.

Ephemeris data tells the GPS receiver where each GPS satellite should be at any time throughout the day. Each satellite transmits ephemeris data showing the orbital information for that satellite and for every other satellite in the system.

Almanac data, which is constantly transmitted by each satellite, contains important information about the status of the satellite ("healthy" or "unhealthy"), current date and time. This part of the signal is essential for determining a position. The main factors that can degrade the GPS signal and thus affect the accuracy of subscriber positioning include the following:

- *Ionosphere and troposphere group delays* due to effects of multipath occurring in the ionosphere. The GPS system uses a special algorithm that calculates an average amount of delay to partially correct for this type of error.
- *Signal multipath* fading [44] which increases the travel time of the signal, thereby causing errors.
- *Receiver clock errors* occur since a ground-based receiver's built-in clock is not as accurate as the atomic clocks onboard the GPS satellites. Therefore, it may have very slight timing errors.
- *Orbital errors* are also known as ephemeris errors; these are inaccuracies of the satellite's reported location.
- *Number of satellites visible* means that the more satellites a GPS receiver can "watch", the better the accuracy. Some strong plasma irregularities may partly block signal reception, causing position errors or possibly no position reading at all. Moreover, ground-based obstructions (buildings, hills, sea, soil etc.) can fully block records from satellite. Therefore, GPS units typically do not work in indoor, underwater or underground environments. The same difficulties with recording of signals occur during such natural disasters, as magnetic storms.

- *Satellite geometry* is referred to the relative position of the satellites at any given time. Ideal satellite geometry exists when the satellites are located at wide angles relative to each other. Poor geometry results when the satellites are located in a line or in a tight grouping.

Typical GPS positioning accuracy was estimated as $15m$ [43, 44]. Typical GPS accuracy of user position is 3-5m and typical Wide Area Augmentation System (WAAS) position accuracy is less than $3m$. Of course, these estimations are correct only in outdoor environments and for regular and non-disturbed ionospheric and atmospheric conditions. Existance of natural or man-made disturbances of the ionosphere decreases essentially the accuracy of subscriber positioning. Thus, the accuracy of the original GPS system, which was subject to accuracy degradation under the Selective Availability Program (USA), is $100m$.

In other countries were developed similar satellite-based differential systems. In Asia, this is the Japanese Multi-Functional Satellite Augmentation System (MSAS), while Europe has the Euro Geostationary Navigation Overlay Service (EGNOS). Eventually, GPS users around the world will have access to precise position data using these and other compatible systems. The Russian GLONASS is a Global Navigation Satellite System in the process of being restored to full operation. The European Union's Galileo positioning system is a next generation of GNSS is in the initial deployment phase, scheduled to be operational in 2010. China has indicated it may expand its regional Beidou navigation system into a global system at the same time. India's IRNSS, a next generation GNSS is in developmental phase and is scheduled to be operational only around 2012.

GPS ionospheric sounding is a powerful tool for remote sensing of the ionosphere. GPS radio signals L1 and L2 have provided an unique opportunity to study: short scale length variations in Total Electron Content (TEC) along the signal path in the presence of ionospheric irregularities and scintillations caused by these irregularities (GPS based ionospheric measurement can measure TEC variations smaller than 10^{-2} TEC units) [45, 46, 47]; isolated ionospheric disturbances [48]; simulation of the ionospheric disturbances caused by earthquakes, explosions, cyclones, and tsunamis [49, 50]; variations of atmospheric water vapour [51]; ground complex permittivity [52]; processors of horizontal and vertical crustal deformation [53]; influences of the ionosphere on satellite communications and satellite measurements; and so on.

In [45] was demonstrated the use of GPS in obtaining profiles of electron density and other geophysical variables such as temperature, pressure and water vapour in lower ionosphere. This work presents a set of ionospheric profiles obtained from GPS/MET with the Abel inversion technique. The effects of the ionosphere on the GPS signal during occultation, such as bending and scintillation, was also examined in [45]. Electron density profiles obtained from GPS/MET are compared with the ones obtained from the Parameterized Ionospheric Model (PIM) and with ionosonde and incoherent scatter radar measurements. Statistical comparisons of $Nm F2$ values obtained from GPS/MET and ionosondes indicate that these two types of measurements are obtained with accuracy of about 20%.
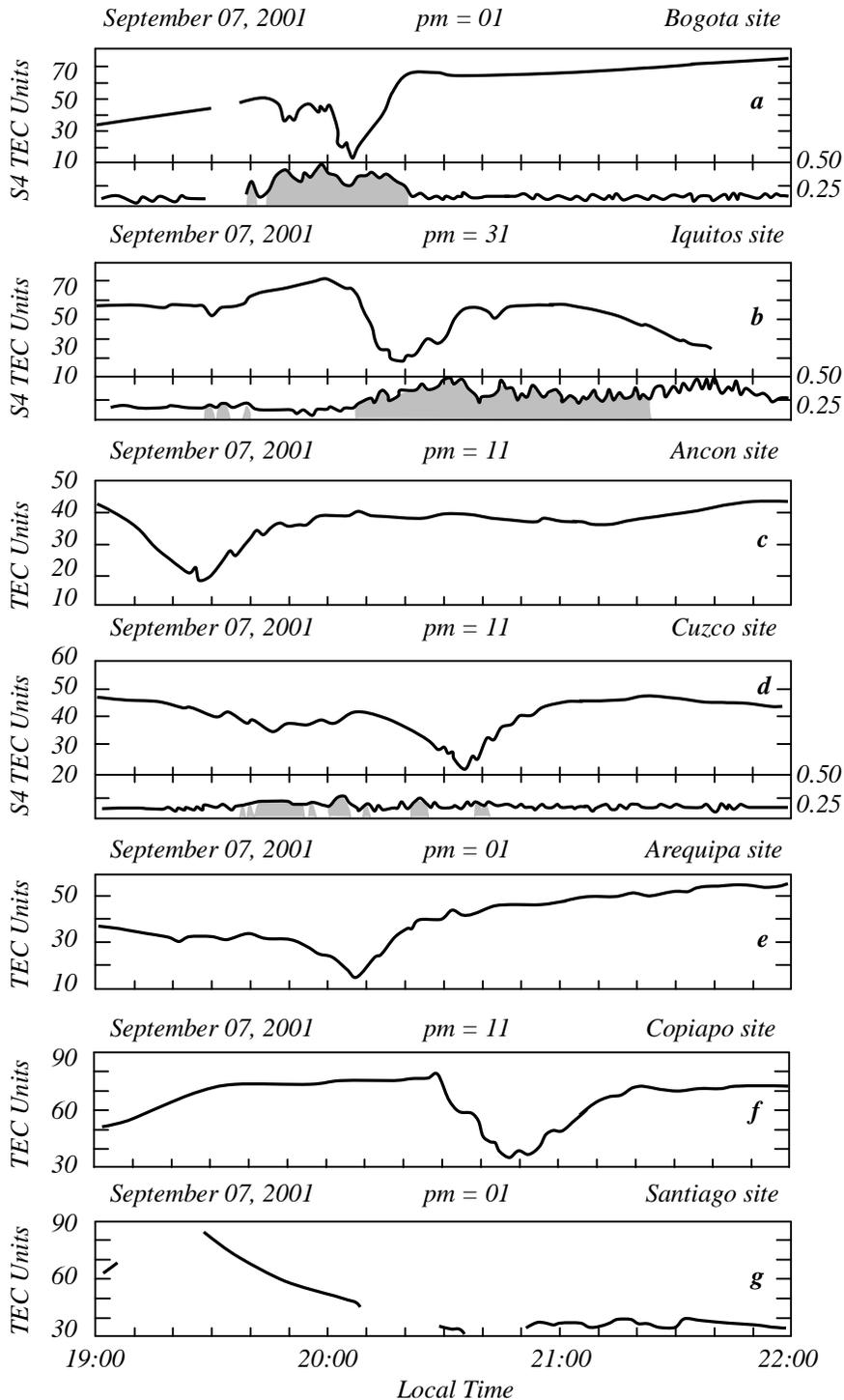
Fig. 13. Values of absolute TEC measured at several sites using signals from 3 GPS satellites. In all of this passes TEC depletions are evident, sometimes exceeding 50 TEC units (10^{16} el/m^2). The additional sub-panel plotted below the Bogota, Iquitos and Cuzco TEC data corresponds to the S4 GPS scintillation index.

A latitudinal-distributed network of GPS receivers has been operating within Colombia, Peru and Chile with sufficient latitudinal separation for measuring of the absolute TEC at both crests of the equatorial anomaly is presented in [47]. The network also indicated the latitudinal extension of GPS scintillations and TEC depletions. I present here only a characteristic example of measurements carried out in [47].

Thus, Fig. 13 shows TEC depletions measured at several sites, using signals from three different GPS satellites. On September 07, 2001, TEC depletion was observed at all stations except Antuco station. In addition, the receiver at Santiago suffered a loss of signals caused by the strong fading which likely associated with TEC depletions. Figure 13a shows the passage of a TEC depletion, 35 TEC units (10^{16} el/m^2) in depth, detected by the receiver at Bogota between 20:00 and 20:20 LT. Below the TEC curve is displayed with the scintillation index (called S4-index), which was calculated on-line using the signal received from each of GPS satellites. The gray shadowing indicates the times when the S4-index is above the noise level when the satellite elevation is above 20º. The TEC depletion of Fig. 13a is accompanied by high levels of GPS scintillations (S4=0.5) on both the East and West walls of the depletion.

Figure 13b illustrates the same TEC depletion that was detected at Bogota receiver at the time of 11 minutes earlier, but at Iquitos receiver, strong values of the scintillation index (S4=0.5) were observed only on the West wall and weaker scintillations on the East side (S4=0.25) of the depletion. Due to smaller angle of observation, the receiver at Iquitos receiver observed the same TEC depletion that was obtained at Bogota receiver with an apparent wider width. The authors of [47] used the transit time of TEC depletions between Ancon receiver and Cuzco receiver of about $65min$, which were separated by $550km$-range in the magnetic East-West direction. They also estimated a 140-m/s zonal drift.

Scintillations at Cuzco receiver (Fig. 13d) were of less intensity, due to a smaller density that commonly prevails near the magnetic equator when the anomaly is fully developed. At Arequipa receiver, the lowest value within the TEC depletion was observed at 20:08 UT. This is the same time that the minimum TEC was detected at Bogota receiver (see Fig. 13a), which is located $225km$ westward and several hundred kilometers northward from Arequipa receiver. This apparent discrepancy can be explained if we allow the bubbles to tilt westward at altitudes above the *F*-region peak. The westward tilt will make the part of the TEC depletions that extend to higher latitudes to appear at slightly later times in a way similar to the plasma plumes seen with coherent radars. The Copiapo receiver (Fig. 13f) detected a 30-TEC-unit depletion spanning between 20:30 and 21:10 LT.

Developments of LFM Ionosondes in the Historical Perspective

In the recent decades in different regions of the world, active scientific studies of the ionospheric physics and ionospheric radio propagation were carried out based on local ground-based networks, called *LFM-ionosondes*, which started

intensively to be used also for selection of the optimal ionospheric radio channels. This relates to the fact that LFM ionosondes have advantages compared to pulse ionosondes, such as a high defence against noise and high electromagnetic compatibility (thus, the radiated power is only about 2W to 100W), as well as smaller dimensions of the facility.

Special signals with LFM were first used for the purpose of radiolocation [54] and then, in 1954, for the sounding of the ionosphere in regions with high absorption, about 80-90dB. Later, in 1962, such signals were used for investigation of *D*-layer of the ionosphere [55-57].

Theoretical aspects of radiation and recording of pulse LFM signals have found their application after creation of methods and approaches dealing with generation of LFM signals. The first tests showed immediately high efficiency of LFM ionosondes for vertical and oblique sounding of the ionosphere [61]. In [62] the experimental ionospheric sounding, vertical and/or oblique, was presented, using the frequency range from 600 kHz to 2 MHz. The equipment employs a linear frequency sweep transmission generated by direct synthesis from a frequency standard. An identical sweep is used for demodulation at the receiver. Sounding records were obtained at night-time periods along the 2000-*km* radio paths. Radiated power was ranged from 25W to 250W. A good time delay resolution together with suppression of interfering signals makes it possible for ionospheric sounding with a greatly improved quality of transmission of any information at large distances using low energy of the transmitting signals.

For applied studies, during 1960s special systems were performed, operating at the continuous LFM signals [63]. The study of the ionosphere with these systems allowed to obtain a set of original results described in [64, 65]. Further, great success in creation of LFM ionosondes was achieved by "Barry Research" Company (USA), the typical models of ionosondes of which for vertical sounding (VS) and oblique sounding (OS) of the ionosphere, VOS–1 [66], RCS–2 [67], and RCS–4 [68], allowed to obtain ionograms of high quality using very low radiation power, of about 5-10W only. At present, this company has begun to produce LFM transivers XCS-6 and TST 4280.

During the period from 1980 to 2000, in different regions of the world the high-effective systems were realized for investigation of the ionosphere, as well as developments of new methods of diagnostics of short-wave ionospheric radio channels, including prediction of the working frequencies (called *maximum useful frequencies*, MUF) of radio communication links and also service of short-wave over-horizon radars [57]. Modification of the standard LFM ionosonde of "Barry Research" Company (see [71, 72]) by introducing multi-channel record with digital registration and signal processing, allows to create a monostatic ionosonde of vertical sounding with registration of arriving angles, with estimation of polarization and Doppler speed of displacement points of wave reflection.

A bistatic LFM ionosonde was constructed in England to study dispersion distortions of wideband signals at the short-length radio traces [73, 74]. A set of experiments at the one-hop traces in the polar and equatorial ionosphere was

carried out to investigate the effects of ionospheric irregularities on radio scattering phenomena [75].

"TCI/BR Communications" corporation has carried out a global experiment using 16 LFM ionosondes to provide and secure radio communication at the short-frequency band. They used data obtained from 30 radio traces of oblique sounding [76]. The same European project was made at two radio traces using ionosondes of the company "BR Communications" [77, 78].

For the study of "thin" ionospheric effects in the propagation of short-wave radio signals, the research groups "Defense Evaluation" and "Research Agency" (DERA, UK) created a high-quality ionosonde for oblique sounding, called Improved Radio Ionospheric Sounder (IRIS) [79, 80]. In 1992, at South-West Research Institute (San Antonio, USA) a small multi-channel interferometer was developed on the basis of an LFM ionosonde for measurements of group delay and angles-of-arrival in the azimuthal and elevation local planes [81]. Over-horizon radars of short-wave frequency band also used LFM signals for ionospheric diagnostics and to testing the accuracy of ionospheric models, as well as conditions of the ocean surface and ocean flows [82–85].

Australian Defence Science and Technology Organisation created in Australia a wide net of ionosondes of oblique sounding to investigate the low-latitude ionosphere and to ensure a stable operation of an over-horizon short-wave radio locator [86-88]. A net of LFM-ionosondes of the IPS-71 type, produced by the Australian company "KEL Aerospace Pty Ltd", situated on the territory of Australia, includes ionosondes for vertical and oblique sounding of the ionosphere. Such ionosondes have the velocity of frequency changes of 500 *kHz/s*. Studies of the peculiarities of the low-latitude ionosphere above the Asian-Pacific-Ocean region [88] are carried out using LFM ionosondes developed by Australian Defense Science and Technology Organization (DSTO).

In [87], the technique that uses for the measurements of the time-varying narrowband (10 kHz) component-transfer function of a high-frequency (HF) frequency-modulated (FM) continuous wave, transmitted at 15.085 MHz, and its decomposition into propagation modes, is presented. One event occurring at a 5244-*km* transmission path, which exhibits flat fading within the 10-*kHz* bandwidth, is analyzed and found to exhibit severe phase distortion due to multipath. A component-transfer function for an individual propagation mode was also obtained in [87] using two-dimensional filtering of the signal in the joint Doppler frequency (DF) and time delay (TD) domain, resulting in a significant reduction in phase distortion.

In former USSR, was first constructed an ionosonde for vertical sounding (VS) of the ionosphere which used quasi-continuous FM signals [57, 89]. Then, ionosondes for VS of the ionosphere were created on the basis of syntezators of continuous LFM signals and their different modifications for VS and OS of the ionosphere [90-96]. With their help, the studies of frequency effects of modification of the ionosphere with powerful short-wave signals were made, as well as long-term investigations of the conditions of propagation of continuous

LFM signals at radio traces of various orientations and lengths [97-100]. Now in Russia an experimental net of LFM ionosondes is operated for oblique sounding (OS) of the ionosphere, the software-hardware methodology of which was developed by several groups [57, 98-100] including a group working at Moldavian Radio Observatory [99, 100].

To secure a stable communication at the short-wave band between countries of NATO, a global net of LFM ionosondes over the world was arranged based on the system AN/TRQ-35(V) (Tactical Frequency Sounding System), which includes 77 transmitters [57]. The AN/TRQ-35(V) is an ionospheric sounding system that easily operates with ionospheric propagation statistics on real-time basis. The system is used to minimize outages related to unpredictable changes of ionospheric characteristics and conditions. It is intended to improve frequency management and assignments of frequencies for HF communications systems, and finally, results in more effective and efficient utilization of the HF spectrum, producing more reliable HF communication with improved grade of service.
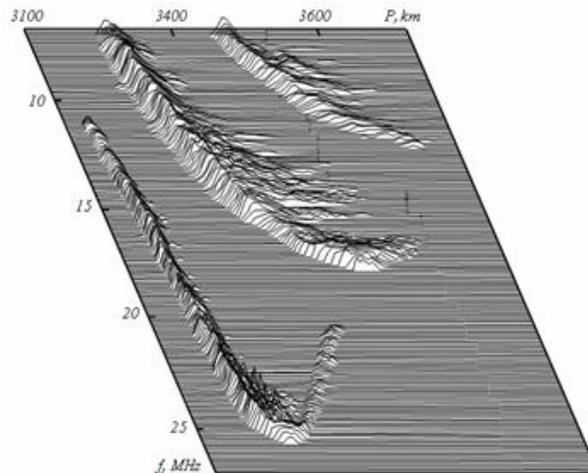

Fig. 14. The experimental amplitude spectrum obtained on the trace Ioscar-Ola-Balti.

Depending on the method of utilization of LFM ionosondes, it is possible to divide them into LFM ionosondes of vertical sounding (VS), oblique sounding (OS) and back-oblique sounding (BOS) [57]. Ionosondes of VS are used mostly to monitor the ionosphere above the local place of the ground-based diagnostic system, as well as to study physical processes occurring during natural and artificial perturbations of the ionosphere [101]. The ionosondes of OS are used mostly to study the ionosphere along the trace of short-wave radio propagation under various geographic conditions in adaptive communication systems and to secure frequency during selection of the optimal radio channel [82, 101, 104]. Ionosondes of BOS are used to study propagation conditions in the ionosphere [83–85] and to investigate conditions of sea surface in the large spatial regions, as well as in the systems of frequencies securing in short-wave radio communication channels and over-horizon short-wave radars [86].

As an illustration, in Fig. 14 the experimental amplitude spectrum $|S_k(t)|$ is presented during sounding on the trace Ioscar-Ola-Balti on December 10, 1991. The group path $P=ct$ is arranged along the axis of delays. The registered signals correspond to bottom and top rays of one-, two- and three-hope modes of propagation. The graphical imaging of the cross-section of $|S_k(W)|=|S_k(t)|$ at the given level presents an actual ionogram of oblique sounding. The dependence $|S_k(t)|$ at the time t_k presents the amplitude relief of the signal at the current frequency f_k for all the registered modes of propagation.

Conclusion

The parameters and dynamical processes occurring in the non-regular ionosphere are possible to investigate using modern radiophysical methods based on different devices and radio systems, such as optical devices, incoherent scatter radars, Global Navigation Satellite Systems, superDARN, ionosondes, and digisondes.

1. Optical devices, such as photometric and spectrometric devices, digital All - Sky cameras, and TV complexes are used to investigate the atmospheric and ionospheric parameters and processes separately or with radar systems and ionosondes, operating regularly in many places over the world, such as Alaska, Arecibo, Arequipa, Fairbanks, New Zealand, Peru and Puerto Rico, Russia, the North and South Pole.

2. Photometers, combined with a set of optical filters, are used to measure the intensities of airglow emissions of the visible and near-infrared part of the optical spectrum of various gases in the atmosphere, such as OH, O_2, O, O^+, N, N_2^+, H, He, and Na.

3. Spectrometers are used to measure spectral blends of airglow emission bands at medium to high spectral resolution. For example, the Ebert-Fastie Spectrophotometer arranged at AISRS has the following parameters: one-meter focal length with a bandwidth varied between 0.02 nm to 1.0 nm. A programmable wavelength scanning takes place via stepping motors with maximum scan range limited to 100nm (anywhere between roughly 300nm and 900 nm) with variable field-of-view, which varies between 0.1^o and 9.0^o.

4. Interferometers are generally used to measure Doppler temperature and winds that originate in the E- and F-regions of the ionosphere, or to measure the spectral distribution and temporal variation of the hydrogen geocorona [5–7]. Fabry-Perot Interferometers at AISRS have the following parameters: each interferometer is with 1.2-meter focal length and 0.15-meter clear apertures with typical bandwidth of 0.001nm and free spectral range of 0.01nm. The wavelength change takes place via pressure scanning using pistons and choice of scanning gas of Ar, CO_2, or SF_6. The field-of-view depends on the choice of aperture size, but it is typically 0.25^o for 630nm observations.

5. The Doppler Rayleigh Lidar is used to measure the Doppler shifts and widths of the spectrum of the laser light that is broadened and backscattered from the

atmosphere and lower ionosphere from about 15 to 70-80 km of altitude. The Doppler Rayleigh Lidar, for example, has the following parameters: Nd/YAG-based laser transmitter with the 24-W average power (with 100 MW in its peak) operating at 532 nm and at frequency of 40 Hz with the pulse width of 6ns.

6. The all-sky camera systems are used to simultaneous imaging observations of several airglow layers. These are very important to study vertical propagation of atmospheric gravity waves, which is one of the main aspects in bubbles structures generation in the equatorial layer *F*.

7. Incoherent Scatter Radar is a technique for detecting and studying remote targets by transmitting a radio wave in the direction of the target, observing the reflection of the wave and providing the direct information about electron densities, line-of-sight drift velocities, the height of ionospheric layers and ratio electron and ion temperatures, T_e / T_i. They also provide indirect measurements of a number of additional parameters, the most reliable of which is the neutral wind below ionospheric altitudes of 130*km*.

8. The Super Dual Auroral Radar Network is an international system for the studying of the Earth's upper troposphere, ionosphere, and their connections with the magnetosphere and outer space surrounding the Earth, which currently consists of a set of radars in the northern and in the southern hemispheres.

9. GPS has become a widely used aid to navigation worldwide, and a useful tool for map-making, land surveying, commerce, and scientific uses. GPS also provides a precise time reference used in many applications including scientific study of earthquakes, and synchronization of telecommunications networks.

10. The GPS radio signals L1– 1575.42 MHz and L2– 1227.60 MHz have provided an unique opportunity to study the next ionospheric parameters and phenomena's: short scale length variations in Total Electron Content along the signal path in the presence of ionospheric irregularities and scintillations caused by these irregularities (GPS based ionospheric measurement can measure Total Electron Content variations smaller than 10^{-2} TEC units); isolated ionospheric disturbances; simulation of the ionospheric disturbances caused by earthquakes, explosions, cyclones, and tsunamis; variations of atmospheric water vapour; ground complex permittivity; processors of horizontal and vertical crustal deformation; influences of the ionosphere on satellite communications and satellite measurements.

11. In different regions of the world, active scientific studies of the ionospheric physics and ionospheric radio propagation were carried out based on local ground-based networks, called LFM-ionosondes, which started intensively to be used also for selection of the optimal ionospheric radio channels. LFM ionosondes have advantages compared to pulse ionosondes, such as a high defence against noise and high electromagnetic compatibility (thus, the

radiated power is only about 2W to 100W), as well as smaller dimensions of the facility.

12.   It is possible to divide LFM ionosondes into LFM ionosondes of vertical sounding, oblique sounding and back-oblique sounding. Ionosondes of vertical sounding are used mostly to monitor the ionosphere above the local place of the ground-based diagnostic system, as well as to study physical processes occurring during natural and artificial perturbations of the ionosphere. The ionosondes of oblique sounding are used mostly to study the ionosphere along the traces of short-wave radio propagation under various geographic conditions in adaptive communication systems and to secure frequency during selection of the optimal radio channel. Ionosondes of back-oblique sounding are used to study propagation conditions in the ionosphere and to investigate conditions of sea surface in large spatial regions, as well as in the systems of frequencies securing in short-wave radio communication channels and over-horizon short-wave radars.

Bibliography

1.   Mende, S. B., R. H. Eather, M. H. Rees, R. R. Vondrak, and R. M. Robinson, *Optical mapping of ionospheric conductance*, J. Geophys. Res., vol. 89, 1984, pp. 1755-1763.

2.   Robinson, R. M., S. B. Mende, R. R. Vondrak, J. U. Kozyra, and A. F. Nagy, *Radar and photometric measurements of an intense type a red Aurora*, J. Geophys. Res., vol. 90, 1985, pp. 457-466.

3.   Bird, J. C., G. G. Shepherd, and C. A. Tepley, *Comparison of lower thermospheric winds measured by a polarizing Michelson interferometer and a Fabry-Perot spectrometer during the AIDA campaign*, J. Atmos. Terr. Phys., vol. 55, 1993, pp. 313-324.

4.   Feldman, P. D., D. J. Sahnow, J. W. Kruk, E. M. Murphy, and H. W. Moos, *High resolution FUV spectroscopy of the terrestrial day airglow with the far ultraviolet spectroscopic explorer* , J. Geophys. Res., vol. 106, 2001, pp. 8119-8130.

5.   Wickwar, V. B., J. W. Meriwether, P. B. Hays, and A. F. Nagy, *The meridional thermospheric neutral wind measured by radar and optical techniques in the auroral region*, J. Geophys. Res., vol. 89, 1984, pp. 10, 987-10, 998.

6.   Burnside, R. G., and C. A. Tepley, *Optical observations of thermospheric neutral winds at Arecibo between 1980 and 1987*, J. Geophys. Res., vol. 94, 1989, pp. 2, 711-2, 716.

7.   Kerr, R. B., R. P. Cageao, C. A. Tepley, S. K. Atreya, and T. M. Donahue, *High spectral resolution Fabry-Perot interferometer measurements of Comet Halley at H-alpha and 6300 Å*, Adv. Space Res., vol. 5, 1986, pp. 283-287.

8.   Tepley, C. A., S. I. Sargoytchev, and C. O. Hines, *Initial Doppler Rayleigh lidar results from Arecibo*, Geophys. Res. Lett., vol. 18, 1991, pp. 167-170.

9. Tepley, C. A., *Neutral winds of the middle atmosphere observed at Arecibo using a Doppler Rayleigh lidar*, J. Geophys. Res., vol. 99, 1994, pp. 25,781-25,790.

10. Beatty, T. J., R. L. Collins, C. S. Gardner, et al., *Simultaneous radar and lidar observations of sporadic E and Na layers at Arecibo*, Geophys. Res. Lett., vol. 16, 1989, pp. 1,019-1,022.

11. Friedman, J. S., C. A. Tepley, P. A. Castleberg, and H. Roe, *Middle-atmospheric Doppler lidar using an iodine-vapor edge filter*, Optics Letters, vol. 22, 1997, pp. 1,648-1,650.

12. Friedman, J. S., C. A. Tepley, S. Raizada, et al., *Potassium Doppler-resonance lidar for the study of the mesosphere and lower thermosphere at the Arecibo Observatory*, J. Atmos. Solar Terr. Phys., vol. 65, 2003, pp. 1411-1424.

13. Grime, B. W., T. J. Kane, S. C. Collins, M. C. Kelley, et al., *Meteor trail advection and dispersion: Preliminary lidar observations*, Geophys. Res. Lett., vol. 26, 1999, pp. 675-678.

14. Hecht, J. H., T. J. Kane, R. L. Walterscheid, C. S. Gardner, and C. A. Tepley, *Simultaneous nightglow and Na lidar observations at Arecibo during the AIDA-89 campaign*, J. Atmos. Terr. Phys., vol. 55, 1993, pp. 409-423.

15. Kane, T. J., C. S. Gardner, Q. Zhou, J. D. Mathews, and C. A. Tepley, *Lidar, radar and airglow observations of a prominent sporadic Na / sporadic E layer event at Arecibo during AIDA-89*, J. Atmos. Terr. Phys., vol. 55, 1993, pp. 499-511.

16. Raizada, S., C. A. Tepley, D. Janches, et al., *Lidar observations of Ca and K metallic layers from Arecibo and comparison with micrometeor sporadic activity*, J. Atmos. Solar Terr. Phys., vol. 66, 2004, pp. 595-606.

17. Shiokawa, K., Y. Katoh, M. Satoh, et al., *Development of optical mesosphere thermosphere images (OMTI)*, Earth Planets Space, vol. 51, 1996, pp. 887-896.

18. Zhou, Q., J., and Y. T. Morton, *A case study of mesospheric gravity wave momentum flux and dynamical instability using the Arecibo dual beam incoherent scatter radar*, Geophys. Res. Lett., vol. 33(10), doi: 10.1029/2005GL025608, 2006.

19. Wen, C. H., J. F. Doherty, J. D. Mathews, and D. Janches, *Meteor detection and non-periodic bursty interference removal for Arecibo data*, J. Atmos. Solar Terr. Phys., vol. 67, 2005, pp. 275-281.

20. Luan, X., L. Liu, W. Wan, et al., *A study of the shape of topside electron density profile derived from incoherent scatter radar measurements over Arecibo and Millstone Hill*, Radio Sci., vol. 41(4), doi:10.1029/2005RS003367, 2006.

21. Hysell, D. L., *Incoherent scatter experiments at Jicamarca using alternating codes*, Radio Sci., vol. 35, 2000, pp. 1425-1435.

22.   Woodman, R. F., and J. L. Chau, *Equatorial quasiperiodic echoes from field-aligned irregularities observed over Jicamarca*, Geophys. Res. Lett., 28, 2001, pp. 207-209.

23.   Hysell, D.L.; and J. D. Burcham, *Long term studies of equatorial spread F using the JULIA radar at Jicamarca*. J. Atmos. Solar-Terr. Phys., vol. 64, 2002, pp. 1531-1543.

24.   Caudal, G., O. de la Beaujardière, D. Alcaydé, J. Holt, and G. Lejeune, *Simultaneous measurements of the electrodynamic parameters of the auroral ionosphere by the EISCAT, Chatanika, and Millstone Hill Radars*, Ann. Geophys., vol. 2, 1984, pp. 369-376.

25.   Lockwood, M., I. W. McCrea, G. H. Millward, R. J. Moffett and H. Rishbeth, *EISCAT observations of ion composition and temperature anisotropy in the high-latitude F-region*, J. Atmos. Terr. Phys., vol. 55, 1993, pp. 895-906.

26.   McCrae, I. W., M. Lockwood, J. Moen, et al.. *ESR and EISCAT observations of the response of the cusp and cleft to IMF orientation changes*, Annales Geophysicae, vol. 18, 2000, pp. 1009-1026.

27.   Zhang, S.-R., J. M. Holt, D. K. Bilitza, et al., *Multiple-site comparisons between models on incoherent scatter radar and IRI*, Adv. Space Res., vol. 39, 2007, pp. 910-915.

28.   Lathuillere, C., V. B. Wickwar, and W. Kofman, *Incoherent scatter measurements of ion neutral collision frequencies and temperatures in the lower thermosphere of the auroral region*, J. Geophys. Res., vol. 88, 1983, pp. 10,137-10,144.

29.   Robinson, R. M., F. Rich, and R. R. Vondrak, *Chatanika radar and S32 measurements of auroral zone electrodynamics in the didnight sector*, J. Geophys. Res., vol. 90, 1985, pp. 8487-8499.

30.   Rasmussen, C. E., R. W. Schunk, J. J. Sojka, et al., *Comparison of simultaneous Chatanika and Millstone Hill observations with ionospheric model predictions*, J. Geophys. Res., vol. 91, 1986, pp. 6986-6998.

31.   Hecht, J. H., R. L. Walterscheid, G. G. Sivjee, A. B. Christensen, and J. B. Pranke, *Observations of wave driven fluctuations of OH nightglow emission from Sondre Stromfjord, Greenland*, J. Geophys. Res., vol. 92, 1987, pp. 6091-6099.

32.   Robinson, R. M., C. R. Clauer, O. de la Beaujardière, et al., *Sondrestrom and EISCAT radar observations of polewardmoving auroral forms*, J. Atmos. Terr. Phys., vol. 52, 1990, pp. 411-420.

33.   Johnson, R. M., and T. S. Virdi, *High latitude lower thermospheric neutral winds at EISCAT and Sondrestrom During LTCS 1*, J. Geophys. Res., vol. 96, 1991, pp. 1099-1116.

34.   Kelly, J. D., C. J. Heinselman, J. F. Vickrey, and R. R. Vondrak, *The sondrestrom radar and acoompanying ground-based instrumentation*, Space Science Reviews, vol. 71, 1995, pp. 797-813.

35. Bristow, W. A., and B. J. Watkins, *Incoherent scatter observations of thin ionization layers at sondrestrom*, J. Atmos. Terr. Phys., vol. 55, 1993, pp. 873-894.

36. Sofko, G. J., A. V. Koustov, K. McWilliams, et al., *The super dual auroral radar network (SuperDARN): An international system for space weather determination*, Physics in Canada, vol. 54, 1998, pp. 6-23.

37. Oksavik, K., R. A. Greenwald, J. M. Ruohoniemi, et al., *First observations of the temporal/spatial variation of the sub-auroral polarization stream from the SuperDARN wallops HF radar*, Geophys. Res. Lett., 33, L12104, doi:10.1029/2006GL026256, 2006.

38. Ponomarenko, P. V., F. W. Menk, C. L.Waters, and M. D. Sciffer, *Pc3–4 ULF waves observed by the SuperDARN TIGER radar*, Annales Geophysicae, vol. 23, 2005, pp. 1271–1280, SRef-ID: 1432-0576/ag/2005-23-1271.

39. Pinnock, M and A. S. Rodger, *On determining the noon polar cap boundary from the SuperDARN HF radar backscatter characteristics*, Annales Geophysicae, vol. 18, 2001, pp. 1523-1530.

40. Bristow, W. A., and D. Lummerzheim, *Determination of field-aligned currents using the Super Dual Auroral Radar Network and the UVI ultraviolet imager*, J. Geophys. Res, vol. 106, 2001, pp. 18,577-18,588.

41. Ponomarenko, P. V., and C. L. Waters, *The role of Pc1-2 waves in spectral broadening of SuperDARN echoes from high latitudes*, Geophys. Res. Lett., vol. 30, 2003, pp. 1122-1125.

42. Provan, G., T. K. Yeoman, S. E. Milan, J. M. Ruohoniemi, and R. Barnes, *An assessment of the "map-potential" and "beam-swinging" techniques for measuring the ionospheric convection pattern using data from the SuperDARN radars*, Ann. Geophys, vol. 20, 2002, pp. 191-202.

43. Van Dierendonck, A. J., *Signal specification for the future GPS civil signal at L5*, Proc. of ION Annual Meeting 2000, San Diego, CA, June 26-28, 2000.

44. Shallberg, K., P. Shloss, E. Altashuler, L. Tahmazyan, *WAAS measurement prossesing, reducing the effects of multipath*, Proc. of ION Annual Meeting 2001, Salt Lake City, UT, September 11-14, 2001.

45. Hajj, G. A., and L. J. Romans, *Ionospheric electron density profiles obtained with the Global Positioning System: Results from the GPS/MET experiment*, Radio Sci., vol. 33, 1998, pp. 175-190.

46. Barrile, V., M. Cacciola, F. C. Morabito, and M. Versaci, *TEC measurements through GPS and artificial intelligence*, J. Electromag. Waves Appl. Vol. 20, 2006, pp. 1211-1220.

47. Valladares, C. E., J. Villalobos, R. Sheehan, and M. P. Hagan, *Latitudinal extention of low-lattitude scintillations measured with a network of GPS receivers*, Annales Gheophysical, vol. 22, 2004, pp. 3155-3175.

48. Afraimovich, E. L., E. I. Astafieva, and S. V. Voyeikov, *Isolated ionospheric disturbances as deducted from global GPS network*, Ann. Geophys. vol. 22, 2004, pp. 47-62.

49.   Akhmedov, R. R., and V. E. Kunitsyn, *Simulation of the ionospheric disturbances caused by earthquakes and explosions*, Geomagn. Aeronomy, vol. 44, 2004, pp. 95-101.

50.   Kuo, Y.-H., X. Zou, and W. Huang, *The impact of Global Positioning System data on the prediction of an extratropical cyclone: an observing system simulation experiment*, Dynamics of Atmospheres and Oceans, vol. 27, 1998, pp. 439-470.

51.   Emardson, T. R., G. Elgered, and J. M. Johansson, *Three months of continuous monitoring of atmospheric water vapor with a network of Global Positioning System receivers*, J. Geophys. Res., vol. 103, 1998, pp. 1807-1820.

52.   Kavak, A., W. J. Vogel, and G. H. Xu, *Using GPS to measure ground complex permittivity*, Electronics Letters, vol. 34, 1998, pp. 254-255.

53.   Liu, Q., *Time-dependent models of vertical crustal deformation from GPS-leveling data*, Surveying and Land Information Systems, vol. 58, 1998, pp. 5-12.

54.   Kuk Ch., and M. Bornfeld, *Radiolocation Signals. Theory and Applications*, Moscow: Soviet Radio, 1971, 567p.

55.   Gnanaligam, S., and K. Weeks, in: *The Physics of the Ionosphere*, edited by J.A.Ratcliffe, The Physical Society, London, 1955, p.63.

56.   Titheridge, J. E., *The electron density in the lower ionosphere*, J. Atmos. Terr. Phys., vol. 24, 1962, pp. 269–282.

57.   Ivanov,   V. A.,   V. I. Kurkin,   V. E. Nosov,   V. P. Uryadov   and V. V. Shumaev, *Chirp ionosonde and its application in the ionospheric research*, Radiophysics and Quantum Electronics, vol. 46, 2003, pp. 821-851.

58.   Klauder, J. R., A. C. Price, S. Darlington, and W. J. Albersteim, *The theory and design of chirp radars*, Bell Syst. Tech. J., vol. 39, 1960, pp. 745-820.

59.   Fenwick, R. B., and G. H. Barry, *Step by step to a linear frequency sweep*, Electronics, vol.38, 1965, pp. 66-67.

60.   Barry, G. H., and R. B. Fenwick, *Extraterrestrial and ionospheric sounding withsynthesized frequency sweeps*, Hewlett-Packard J., vol. 16, 1965, pp. 8-12.

61.   Epstein, M. R., *Polarization of ionospherically propagated HF radio waves with applications to radio communication*, Radio Science, vol.4, 1969, pp. 53-61.

62.   Fenwick, R. B., G. H. Barry, *Sweep-frequency oblique ionospheric sounding at medium frequencies*, IEEE Trans., vol. BC-12, 1966, pp. 25-27.

63.   Croft, T. A., *Sky-wave backscatter: A means for observing our environment at great distance*, Reviews of Geophysics and Space Physics, vol.10, 1972, pp. 73-155.

64.   Barnum J. R. *Skywave polarization rotation in swept-frequency sea backscatter*, Radio Sci., vol.8, 1973, pp. 411-419.

65.   Washburn T. W., L. E. Sweney, J. R. Barnum, and W. B.   Zavoli, *Development of HF skywave radar for remote sensing application.- Special*

topics in HF Propagation, AGARD Conf. Proc. No. 263, 28,05-1.06.1979, London, 32/1-32/17, New York, 1979.

66. *The new VOS-1 vertical/ oblique sounder*, Prospect "Barry Research" Palo Alto, Calif., USA, 1970.

67. *Chirpsounder receiver systems*, Prospect "Barry Research" Palo Alto, Calif., USA, 1972.

68. *Ionospheric chirpsounder transmitter TCS-4*, Prospect "Barry Research" Palo Alto, Calif., USA, 1973.

69. *HF chirpsounder receiver dodel RCS-5*, Prospect "BR Communications", USA, 1985.

70. *HF chirpsounder transmitter model TCS-5*, Prospect "BR Communications", USA, 1990.

71. Poole, A. W. V., *Advanced sounding (1): The FM-CW alternative*, Radio Sci., vol. 20, 1985, pp. 1609–1616.

72. Poole, A.W.V., and G. P. Evans, *Advanced sounding (2): first results from an. advanced chirp ionosondes*, Radio Sci., vol. 20, 1985, pp. 1617–1623.

73. Salous, S., and E. D. R. Shearman, *Wideband measurements of coherence over an HF skywave link and implication for spread-spectrum communication*, Radio Sci., vol. 21, 1986, pp. 463-472.

74. Salous, S., *FMCW channel sounder with digital processing for measuring the coherence of wideband HF radio links*, IEE Proc., vol.133, Pt. F. 1986, pp. 456-462.

75. Basler, R. P., G. H. Price, R. T. Tsunoda, and T. L. Wong, *Ionospheric distortion of HF signals*, Radio Sci., vol.23, 1988, pp. 569-579.

76. Goodman J. M., Ballard J. W., Sharp E. D., and Trung Luong, *Proc. of Session G5 at the XXVth GA URSI*, Published WDC-A, Boulder, 1998, pp. 64-70.

77. Bröms, M. and B. Lundborg, *Results from Swedish oblique soundings campaigns*, Annali di Geofisica, vol. 37, 1994, pp. 145-152.

78. Lundborg, B., M. Broms, and H. Derblom, *Oblique sounding of an auroral ionospheric HF channel*, J. Atmos. Terr. Phys., vol.57, 1995, pp. 51-63.

79. Arthur, P. C., M. Lissimore, P. S. Cannon, and N. C. Davies, *Application of a high quality ionosonde to ionospheric research*, Proc. of Seventh International Conference on HF Radio Systems and Techniques, IEE Conf. Publ., No. 441, 1997, pp. 135-139.

80. Arthur, P. C. and P. S. Cannon, *ROSE - A high performance oblique ionosonde providing new opportunities for ionospheric research*, Annali di Geofisica, vol. 37, 1994, pp. 135-144.

81. Black, Q. R., J. F. Wood, Jr., A. G. Sonsteby, and W. M. Sherrill, *A direction finding ionosondes for ionospheric propagation research*, Radio Sci., vol. 28, 1993, pp. 795-809.

82. Millman, G. H. and R. W. Swanson, *Comparison of HF oblique transmissions with ionospheric predictions*, Radio Sci., vol. 20, 1985, pp. 315-318,

83.   Anderson, S. J., and M. L. Lees, *High-resolution synoptic scale measurement of ionospheric motions with the Jindalee sky wave radar*, Radio. Sci., vol. 23, 1988, pp. 265-272.

84.   Russell, C. J., P. L. Dyson, Z. Houminer, J. A. Bennett, and L. Li, *The effect of large-scale ionospheric gradients on backscatter ionograms*, Radio Sci., vol. 32, 1997, pp. 1881-1898.

85.   Dandekar, B. S., G. S. Sales, B. Weijers, and D. Reynolds, *Study of equatorial clutter using observed and simulated long-range backscatter ionograms*, Radio Sci., vol. 33, 1998, pp. 1135-1158.

86.   Earl, G. F., and B. D. Ward, *The frequency management system of the Jindalee over-the-horizon backscatter radar*, Radio Sci., vol. 22, 1987, pp. 275–291.

87.   Baker, P.W., R. H. Clarke, A. D. Massie, and D. Taylor, *Techniques for the measurement and decomposition of the time varying narrow bandwidth transfer function of an HF sky wave transmission*, Radio Sci., vol. 32, 1997, pp. 1813-1820.

88.   Lynn, K. J. W., *Oblique sounding in Australia*, INAG-62, 1998, pp. 14-18.

89.   Belenov, A F., V. A. Zinichev, V. A. Ivanov et al., *Sounding of the ionosphere by quasi-continuous signals*, Proc of XIII Conference of Radio Wave Propagation, Gorky, vol.1, 1981, pp. 12-13.

90.   Kochemasov, V. N., L. A. Belov, and V. S. Okoneshnikov, *Formation of Signals with Linear Frequency Modulation*, Moscow: Radio and Communication, 1983, 192p.

91.   Erukhimov, L. M., V. A. Ivanov, N. A. Mityakov, et al., *LFM-Method of Diagnostics of the Ionospheric Channel*, Moscow: VINITI, No. 9027-1386, 1986, 94p.

92.   Ivanov, V. A., V. A. Frolov, and V. V. Shumaev, *Sounding of the ionosphere by continuous LFM signals*, Izv. Vuzov, Radiophyzika, vol. 29, 1986, pp. 235-237.

93.   Brynko, I. G., I. A. Galkin, V. P. Grozov et al., *Automatically controlled data gathering and processing system using an FMCW ionosondes*, Adv. Space Res., vol. 4, 1988, pp. 121-124.

94.   Ivanov, V. A., V. P. Uryadov, V. A. Frolov, and V. V. Shumaev, *Oblique sounding of the ionosphere by continuous LFM-signals*, Geomagn. Aeronomy, vol. 30, 1990, pp. 107-112.

95.   Ivanov, V. A., Yu. B. Malishev, Yu. V. Noga et al., *Automatic LFM-complex for ionospheric studies*, Radiotechnics, No. 4, 1991, pp.69-72.

96.   Filipp N. D., N. Sh. Blaunshtein, L. M. Erukhimov, V. A. Ivanov, and V. P. Uryadov, *Modern Methods of Investigation of Dynamic Processes in the Ionosphere*, Shtiintza, Kishinev, Moldova, 1991, 288p.

97.   Zinichev, V. A., V. A. Ivanov, V. A. Frolov, and V. V. Shumaev, *Use of LFM method of vertical sounding for study of modified upper layers of the ionosphere*, Izv. Vusov. Radiophysika, vol. 29, 1986, pp. 629-631.

98. Erukhimov, L. M., V. A. Ivanov, N. A. Mityakov, et al., *On frequency characteristics of effects of powerful radiation at the ionospheric F-layer*, Izv. Vusov. Radiophysika, vol. 30, 1987, pp. 1055-1065.

99. Filip N., Plohotniuc E., Pascaru M. *Ionosphere prognosis using LFM-ionosound*. Proc. of the XVIII Congress of Româno-American Academy of Science and Arte, Chişinău. Moldova, 1993, vol. 2. pp. 135-137.

100. Ureadov, V., V. Ivanov, E. Plohotniuc, L. Eruhimov, N. Blaunshtein, and N. Filipp, *Dynamic Processes in Ionosphere and Methods of Investigation*, Iasi, Romania, Tehnopress, 2006, 284 p.

101. Boguta, N. M., V. A. Ivanov et al., *Use of LFM ionosonde in adaptive system of Short Wave radio communication*, Radiotechniks, No. 4, 1993, pp. 77-79.

102. Lynn, K. J. W., T. J. Harris, M. Sjarifudin, *Stratification of the F2 layer observed in Southeast Asia*, J. Geoph. Res. - Space Physics, vol. 105, A12, 2000, pp. 27147 – 27156.

103. Eremenko, V. A., L. M. Erukhimov, V. A. Ivanov et al., *Pedersen mode ducting in randomly-stratified ionosphere*, Waves in Random Media, vol. 7, 1997, pp. 531-544.

104. Vertogradov, G. G., V. P. Uryadov, and V. G. Vertogradov, *Monitoring of wave disturbances by method of oblique sounding of the ionosphere*, Izv. Vuzov, Radiophyzika, vol. 49, 2006, pp. 1015-1029.

SISTEME OPTICE ŞI RADIO UTILIZATE PENTRU CERCETAREA IONOSFEREI

Eugeniu Plohotniuc
(Universitatea de Stat "Alecu Russo", Republica Moldova)

Este prezentată o succintă descriere a sistemelor optice şi radio moderne utilizate cu succes pentru cercetarea parametrilor, diverselor tipuri de instabilităţi şi neomogenităţi ale plasmei ionosferice.